The Role of the Brune Spectrum in Earthquake Engineering

M.D. Trifunac

Department of Civil Engineering, University of Southern California, Los Angeles, CA 90089-2531, email: trifunac@usc.edu

ABSTRACT: *The concept of response spectrum was proposed by Biot in 1932 for analysis and design of earthquake-resistant structures. It remained in the academic sphere of research for almost 40 years, finally gaining wide engineering acceptance during the early 1970's. Success in recording large number of excellent accelerograms during the 1971 San Fernando earthquake, and publication of Brune [18] paper marked the beginning of the modern era for the Response Spectrum Method (RSM). This paper outlines the ideas which helped develop the modern RSM and describes the role Brune's Spectrum played in this process.*

Keywords: Earthquake Response Spectra; Brune Spectrum; Spectral amplitudes at long periods

1. Introduction

Since its formulation in 1932, the method of Response Spectrum Superposition [1,2] has evolved and contributed in many ways to the Earthquake Engineering Research and applications. Today, it continues to be one of the common ways for characterization of strong motion amplitudes of actual as well as of design ground motions. Spectral amplitudes can be described by detailed empirical scaling equations [3] which involve essentially all presently known and significant scaling parameters in the description of strong ground motion. Response spectrum amplitudes serve as a basis in description of uniform hazard relative response spectra [4]. Uniform hazard spectra are used in development of probabilistic site specific analyses leading to seismic micro and macro zonation [5-7]. Response spectra are also used in probabilistic determination of envelopes of shear forces and bending moments required for engineering design [8], as well as in assessment of losses for buildings exposed to strong shaking [9,10].

2. Classical Response Spectrum

2.1. Historical Notes

Figure (1) outlines selected milestones of the early work in Earthquake Engineering, the years of "important" earthquakes (from engineering point of view) and the years of the world Conferences of Earthquake Engineering.

In the fall of 1931, Professor Kyoji Suyehiro visited the United States and presented a series of three lectures on Engineering Seismology [11]. His third lecture, entitled "Vibration of Buildings in an Earthquake" is of particular interest for Earthquake Engineering. It seems that the term Engineering Seismology – *Jishin Kogaku* – was first used at this time [12]. Kyoji Suyehiro was the member of Imperial Academy, Professor of Applied Mechanics of Tokyo Imperial University and Director of Earthquake Research Institute. He died on April 9, 1932. Suyehiro lectures made strong and lasting impressions on many American seismologists and engineers who later contributed to the development of Earthquake Engineering.

In the early 1930*s* Professors Theodore von Kármán[1] and Maurice Biot[2] were active in the theoretical dynamics aspects of what would later become known as the response spectrum method in earthquake engineering. These ideas were first outlined in the second chapter of Biot's Ph.D dissertation, defended at Caltech in 1932 and entitled "Vibration of

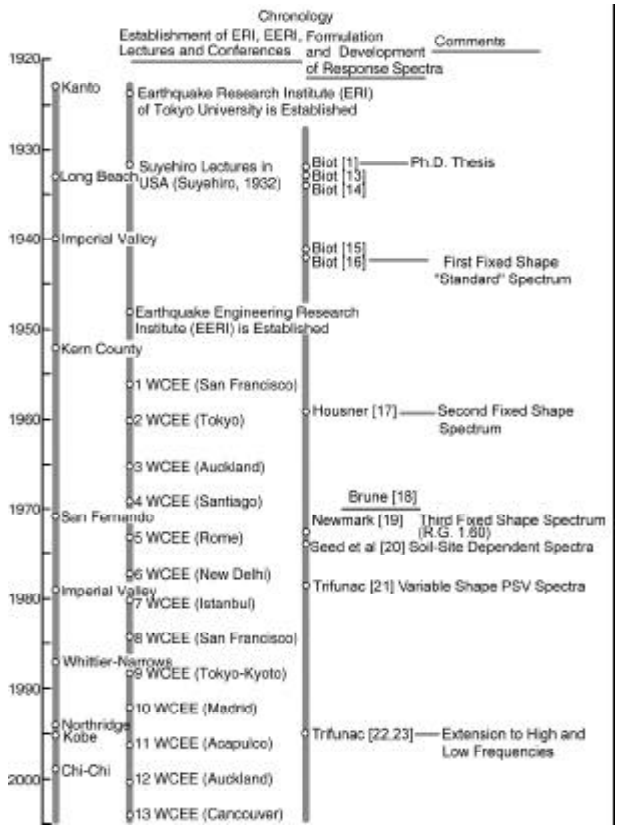

Figure 1. Historical milestones in Earthquake Engineering, with emphasis on the contributions to the subject of Response Spectrum Method. The years of selected earthquakes in Japan and California, and of the establishment of ERI and EERI are also shown.

Buildings during Earthquakes" [1]. Biot's ideas, and further studies undertaken at the suggestion of Professor Theodore von Kármán, were refined while Biot was a Research Fellow at Caltech in 1932 [13,14]. In his 1933 paper, communicated on January 19, 1933, just 50 days before the first strong acceleration was recorded on March 10, 1933 in Long Beach, California, Biot stated: "The study of seismogram spectral distributions has not yet been made; it is, however, the author's opinion that this study would be of great importance for two reasons: (1) The peaks of spectral curves will reveal the presence of certain characteristic frequencies of the soil at a given location. (2) By applying the preceding theorem, the maximum effect of earthquakes on buildings will be easily evaluated…" Biot briefly returned to the subject of earthquake engineering, describing computation of response spectra by a means of mechanical analyzer [15] and formulating the general theory of response analysis and response spectrum superposition [16].

Biot's response spectrum method (*RSM*) was confined to the academic sphere of research for about 40 years, and first started to gain wide engineering acceptance during the early 1970s. There were several reasons for this. First, the computation of response to irregular ground motion was very time consuming and difficult, and there were only a few well-recorded accelerograms that could be used for response studies, see Figure (2). All of this started to change in the mid-1960s, with appearance of digital computers and with commercial availability of strong-motion accelerographs [24,25]. Before the digital computer age, the computation of response was time consuming, and the results were so unreliable that many studies using response spectrum amplitudes from that period must be treated with caution [26]. By late 1960s and early 1970s, the digitization of accelerograms [27] and the digital computation of ground motion and of the response spectra were developed completely and tested for accuracy [28]. Then, in 1970, following publication of Brune's description of the spectra of shear waves [18] (Appendix A), and in 1971, with the occurrence of the San Fernando, California earthquake, the modern era of *RSM* was launched. This earthquake was recorded by 241 accelerographs, including more than 175 from the Los Angeles area, where a large number of instruments had been installed at various levels in high-rise buildings. By combining the data from the San Fernando earthquake with all previous strong motion records, and building on Brune's [18] description of how the spectral shape should depend on stress drop and earthquake magnitude (or seismic moment) it became possible to launch the comprehensive modern empirical scaling analyses of spectral amplitudes [21,29].

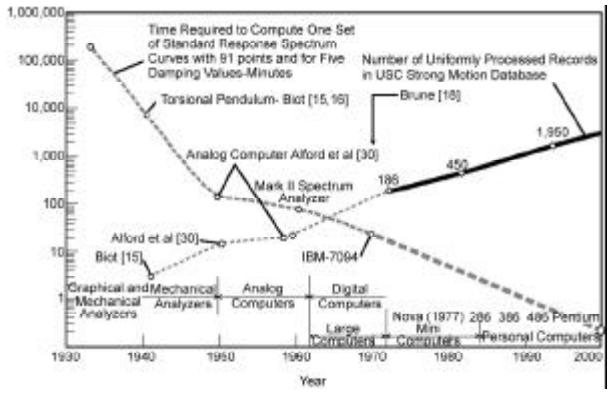

Figure 2. Time required to compute one set of standard response spectrum curves (in minutes), and the cumulative number of accelerograms in strong-motion data bases (light dashed line for the period prior to 1970), and in the uniformly processed strong-motion data base (wide gray line for the period after 1970).

2.2. Fixed-Shape Response Spectra

In his 1934 paper, Biot stated: "If we possessed a great number of seismogram spectra we could use their envelope as a standard spectral curve for the evaluations of the probable maximum effect on buildings." In Biot [15], he continued: "These standard curves … could be made to depend on the nature and magnitude of the damping and on the location. Although the previously analyzed data do not lead to final results, we … conclude that the spectrum will generally be a function decreasing with the period for values of the latter greater than about $0.2s$. A standard curve for earthquakes of the Helena and Ferndale … for values $T > 0.2s$, could very well be the simple hyperbola $A = \frac{0.2g}{T}$ and for $T < 0.2s$, $A = g(4T + 0.2)$, where T is the period in seconds and g the acceleration of gravity. This standard spectrum is plotted in Figures (3) through (6). Whether this function would fit other earthquakes can only be decided by further investigations."

Fifteen years later, Housner averaged and smoothed the response spectra of three strong- motion records from California (El Centro, 1934, $M = 6.5$; El Centro, 1940, $M = 6.7$; and Tehachapi, 1952, $M = 7.7$) and one from Washington (Olympia, 1949, $M = 7.1$). Housner then proposed the use of his average spectrum in design projects, see Figure (3), [17,31]. In engineering design work, the fixed shapes of Housner [31] and Newmark et al [19] spectra (Figures (3) and (4)), normalized to unit peak acceleration, are scaled by selecting the "design" peak acceleration. This procedure, which was first used in the design of nuclear power plants [32], emerged as the "standard" scaling procedure in the late 1960*s* and early 1970*s*, and it is still common today.

2.3. Site-Dependent Spectral Shapes

In one of the first studies to consider the site-dependent shape of spectra, Hayashi et al [33] averaged spectra from 61 accelerograms in three groups (A – very dense sands and gravels; B – soils with intermediate characteristic, and C – very loose soils), and showed that the soil site condition has an effect on the shape of average response spectra. This was later confirmed by Seed et al [34], who considered 104 records and four site conditions (rock, stiff soil, deep cohesionless soil, and soft to medium clay and sand; Figure (5)).

Mohraz et al [35] suggested that the peak ground displacement, d, and peak ground velocity, v, were $d = 36in.$ and $v = 48in./s$ for "alluvium" sites and $d = 12$ in. and $28in./s$ for "rock" sites, both corresponding to a 1g peak ground acceleration. However, because of the small number of recorded accelerograms on rock in 1972, conclusive recommendations on how to describe the dependence of spectra on site conditions were not possible at that time.

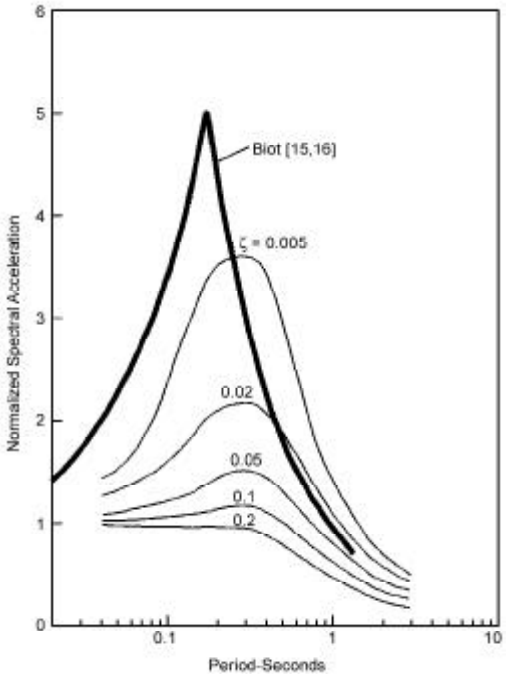

Figure 3. Comparison of Biot [15,16] "standard spectrum" (heavy line) with average spectrum of Housner [17,31].

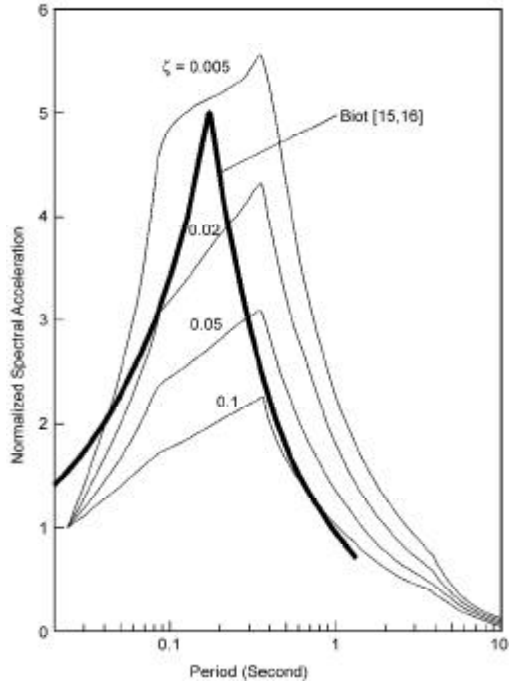

Figure 4. Comparison of Biot [15,16] "standard spectrum" (heavy line) with regulatory guide 1.60 spectrum [32,19].

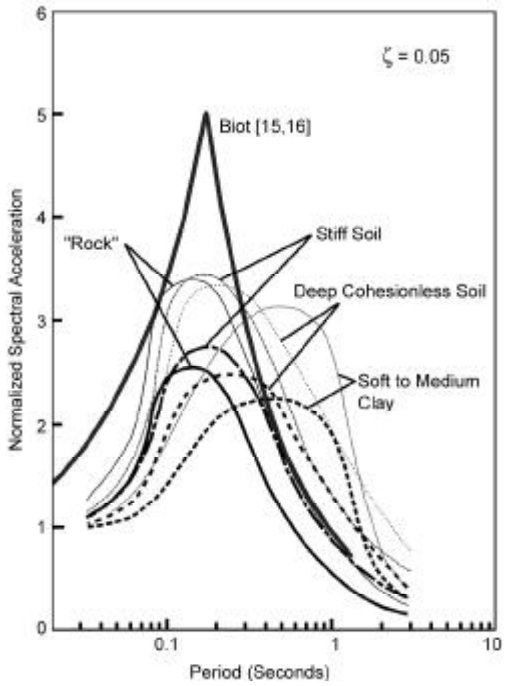

Figure 5. Comparison of Biot [15,16] "standard spectrum" (heavy line) with average (heavy lines) and average plus standard deviation spectra (light lines) of Seed et al [34] for four soil site conditions.

A major and persistent problem in the evaluation of site-dependent spectra of strong earthquake motion is the lack of generally accepted procedures on how to characterize a site. Gutenberg [36] studied the amplification of weak earthquake motions in the Los Angeles area and published the results on average trends and amplification of peak wave amplitudes in sedimentary basins for periods of motion longer than about 0.5*s*. His site characterization could be termed "geological," because he considered the "site" on the scale of kilometers and used the term "rock" to represent geological basement. Twenty years later, Gutenberg's results were shown to be in excellent agreement with the empirical scaling of Fourier amplitude spectra of strong-motion accelerograms of 186 records [29]. While it is clear today that both geotechnical and geological site characterizations must be considered simultaneously [37,38], there is so far no general consensus on how to do this.

2.4. Site-, Magnitude-, and Distance-Dependent Spectra

Publication of Brune's [18] paper (Appendix A) and the occurrence of the San Fernando, California earthquake of 1971 with the large number of new recordings it contributed to the strong-motion database [39,40] opened a new chapter in the empirical studies of response spectra. For the first time, it became possible to consider multi-parameter regressions and to search for the trends in recorded strong-motion data. It became possible to show how spectral amplitudes and spectrum shape change, not only with local soil and geologic site conditions, but also with earthquake magnitude and source-to-station distance, see Figure (6) [21]. During the following 20 years, the subsequent regression studies evolved into advanced empirical scaling equations, contributing numerous detailed improvements and producing a family of advanced, direct scaling equations for spectral amplitudes in terms of almost every practical combination of scaling parameters [37]. The literature on this subject is voluminous, and its review is beyond the scope of this paper. The readers can find many examples and a review of this subject in Lee [3].

Figures (3) through 6 compare Biot's "standard" spectrum shape with other examples of fixed (Figures (3), (4), and (5)) and variable (Figure (6)) spectral shapes. These comparisons are only qualitative, because the methods used in their development and the intended use of the spectral shapes differ. Biot's spectrum was based on the spectra of two

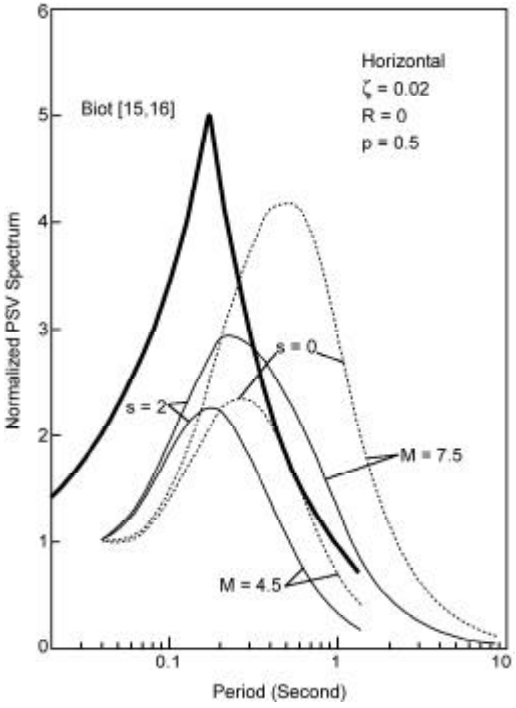

Figure 6. Comparison of Biot [15,16] "standard spectrum" (heavy line) with spectral shapes, which depend upon magnitude (M = 4.5 and 7.5) and geological site conditions (s = 2 for basement rock and s = 0 for sediments), for average spectral amplitudes (p = 0.5), at zero epicentral distance (R = 0) and for 2 percent of critical damping (ζ = 0.02) [21].

earthquakes only (Helena, Montana, 1935, M = 6.0, and Ferndale, California, 1934, M = 6.4). Housner (Figure (3)), Newmark et al [19] (Figure (4)), and Seed et al [34] (Figure (5)) spectra were based on progressively larger numbers of recorded accelerograms (4, 33, and 104, respectively), and on recordings during large earthquakes. Therefore they have broader spectral shapes. The variable shape spectrum, shown in Figure (6), illustrates only the dependence of spectral shape (normalized to 1-g acceleration) on magnitude and geological site conditions. It shows how the spectra broaden with increasing magnitude and how larger magnitudes contribute larger long-period spectral amplitudes.

3. Modern Response Spectra-Empirical Scaling Equations

Modern empirical scaling of response spectrum amplitudes can be traced back to the early 1970's when it become clear that the spectral shape must change with different local site conditions [34], with local geologic site conditions [29], and earthquake magnitude [18]. The more recent empirical equations for scaling the spectral amplitudes now incorporate many additional scaling parameters, and can be presented in terms of earthquake magnitude or local site intensity [41-44]. Here we illustrate only one such scaling equation for pseudo relative velocity spectrum $PSV(T) \equiv \frac{2\pi}{T} SD(T)$, where $SD(T)$ represents the maximum relative displacement of an oscillator with natural period $T=2\pi/\omega$. The empirical scaling equation is [44]

$$\begin{aligned} log_{10}[PSV(T)] = {} & M + Att(\Delta, M, T) + b_1(T)\,M \\ & + b_2(T)\,h + b_3(T)\,v + b_4(T)\,h\,v \\ & + b_5(T) + b_6(T)\,M^2 + b_7^{(1)}(T)\,S_L^{(1)} \\ & + b_7^{(2)}(T)\,S_L^{(2)} \end{aligned} \qquad (3.1)$$

The scaling functions $b_1(T)$ through $b_7^{(2)}(T)$ are determined through a regression analysis of a data base of spectral amplitudes, $PSV(T)$, at 91 discrete periods T ranging from 0.04 sec to 15.0 sec, and for 5 damping values, ζ, equal to 0, 0.02, 0.05, 0.1 and 0.2. The parameters $S_L^{(1)}$ and $S_L^{(2)}$ are indicator variables used to characterize the soil classification at the site, and are defined as

$$S_L^{(1)} = \begin{cases} 1 \text{ if } S_L = 1 \text{ (stiff soil)} \\ 0 \text{ otherwise} \end{cases}$$

and

$$S_L^{(2)} = \begin{cases} 1 \text{ if } S_L = 2 \text{ (deep soil)} \\ 0 \text{ otherwise} \end{cases}$$

The soil classification parameter, S_L, is a qualitative or categorical variable which takes on discrete values of 0, 1 or 2 for three distinct types of soil conditions at the site: "rock" soil, stiff soil and deep soil, [34,38]. M is the earthquake magnitude [45-47] and $Att(D, M, T)$ represents the frequency dependent attenuation versus distance, D. h (measured in kilometers) represents the depth of sediments at the recording site. $v = 0$ for horizontal and $v = 1$ for vertical spectral amplitudes, and $Att(D, M, T)$ takes the form:

$$Att(D,M,T) = \begin{cases} A_o(T)\,log_{10} D & R \le R_o \\ A_o(T)\,log_{10} D_o - \dfrac{(R - R_o)}{200} & R > R_o \end{cases} \qquad (3.2)$$

In Eq. (3.2), D is the representative source-to-station distance given by

$$D = S\left(ln \frac{R^2 + H^2 + S^2}{R^2 + H^2 + S_o^2} \right)^{-1/2}, \qquad (3.3)$$

where R is epicentral distance, H focal depth, and S is source dimension [46,47]. D_o is the corresponding transition source-to-station distance, given by

$$D_o = S\left(ln \frac{R_o^2 + H^2 + S^2}{R_o^2 + H^2 + S_o^2} \right)^{1/2}, \qquad (3.4)$$

and S_o in Eqs. (3.3) and (3.4) is the coherence radius of the source [48]. The term $A_o(T)\,log_{10} D$ is used to calculate the attenuation at distances R less than the transition distance R_o, which is the value of R corresponding to $D_o = D$. For distances $R > R_o$, the attenuation is a linear function of R with slope equal to -1/200. R_o is given by:

$$R_o = \frac{1}{2}\left(\frac{-200\,A_o(T)(1 - S_o^2/S^2)}{ln 10} \right) + \sqrt{\left(\frac{-200\,A_o(T)(1 - S_o^2/S^2)}{ln 10} \right)^2 - 4H^2} \qquad (3.5)$$

and depends on M, H, S, S_o and $A_o(T)$ [49-51].

With $PSV(T)$ representing the pseudo relative velocity response spectrum amplitudes computed from recorded accelerograms, the residues, $\varepsilon(T)$, with respect to the estimates, $\widetilde{PSV}(T)$ (computed from Eq. (3.1)), can be calculated from

$$\varepsilon(T) = log_{10}[PSV(T)] - log_{10}[\widetilde{PSV}(T)]. \qquad (3.6)$$

As in the regression analyses of Fourier and response spectral amplitudes [50], it is assumed that $\varepsilon(T)$ can be described by a probability distribution function of the form:

$$p(\varepsilon,T)=[1-exp(-exp(\alpha(T)\varepsilon(T)+\beta(T)))]^{n(T)} \quad (3.7)$$

where $p(\tilde{\varepsilon},T)$ is the probability that $log_{10}[PSV(T)] - log_{10}[\tilde{PSV}(T)] \le \varepsilon(T)$ at each of the 91 periods T, and $\alpha(T)$, $\beta(T)$, and $n(T)$ are parameters of the distribution function. The integer power $n(T)$ can be estimated from the empirical equation,

$$n(T)=min\left(10,\left[\frac{25}{T}\right]\right) \quad (3.8)$$

with $[\frac{25}{T}]$ representing the integral part of $\frac{25}{T}$. The parameters $\alpha(T)$ and $\beta(T)$ can be estimated from the following equation,

$$ln\left(-ln\left(1-p^{\frac{1}{n(T)}}\right)\right)=\alpha(T)\varepsilon(T)+\beta(T) \quad (3.9)$$

with *ln* denoting the natural logarithm.

The form of Eq. (3.7) results from the assumption that the peak response amplitudes of an oscillator, with small viscous damping, can be approximated by the Rayleigh probability distribution function. The expression for $n(T)$ in Eq. (3.8), derived empirically, and tested in many previous studies, then specifies the number of such peaks that need to be "sampled" to approximate analytically $p(e,T)$, by the expression in Eq. (3.7). This form of $p(e,T)$ was introduced in the late 1970's [21], when it was shown that the residuals of response spectral amplitudes cannot be approximated by a log-normal distribution, by the criteria of χ^2 or Kolmogorov-Smirnov tests.

For a given value of the residue $\varepsilon(T)$ at a particular period T, the actual probability $p^*(e,T)$ that $\varepsilon(T)$ will not be exceeded can be evaluated by finding the fraction of residues $\varepsilon(T)$ (computed from the data at that particular period) which are smaller than the given value. Using Eq. (3.7), the estimated probability $\tilde{p}(\varepsilon,T)$ that $\varepsilon(T)$ will not be exceeded can also be evaluated and compared with $p^*(e,T)$. The Kolmogorov-Smirnov test, $KS(T)$, and the $\chi^2(T)$ test can then be computed to analyze the quality of the fit of the distribution function in Eq. (3.7) [44].

Tables (2.1) (a through e) in Trifunac and Todorovska [53] give $b_1(T)$ through $b_7^{(2)}(T)$ in Eq. (3.1), $M_{min}= - b_1(T)/2b_6(T)$, $M_{max}= (1+ b_1(T))/2b_6(T)$, the functions $n(T)$, $\alpha(T)$, and $\beta(T)$ in Eq. (3.7) and the parameters χ^2 and $KS(T)$. The reader may peruse further details on this model (*MAG-DEPTH-SOIL*) in the paper by Lee [44], where he describes many of the model properties. The reader may study the complete family of Lee's scaling models: 1. *MAG-SITE* [50]; 2. *MAG-DEPTH* [50]; 3. *MAG-SITE-SOIL* [41] and 4. *MAG-DEPTH-SOIL* [44]. In these models, "*MAG*" implies scaling in terms of earthquake magnitude, "*SITE*" indicates use of the geological site parameters, s = 0, 1 or 2 [52], and "*DEPTH*" implies use of the depth of sediments beneath the site, h, in Eq. (3.1). "*SOIL*" indicates that the soil site parameters S_L= 0, 1 and 2 [34,38] are used in the scaling equations. Tables (2.2) (a through e) in Trifunac and Todorovska [53] present the scaling functions in the model *MAG-SITE-SOIL*, where "*SITE*" indicates the use of the geological site conditions in terms of the indicator variables

$$S^{(1)}=\begin{cases}1 & \text{if } s=1 \text{ (basement rock)}\\ 0 & \text{otherwise}\end{cases}$$

$$S^{(2)}=\begin{cases}1 & \text{if } s=2 \text{ (basement rock)}\\ 0 & \text{otherwise}\end{cases}$$

in place of h, as in Eq. (3.1). In the following we will refer to the above four models as "the group of four regression models" or "*G4RM*".

In Figure (7), the light shaded area shows the region where the empirical scaling equation for *PSV* spectra, Eq. (3.1), is valid, up to f = 25*Hz* and for magnitudes $4 \le M \le 8$. The darker shaded area represents the amplitudes of the digitization and processing noise [54] representative of the data which were used in the development of the same equation. In the long period range, Eq. (3.1) is valid up to the cut off periods $T(N_c)$, shown in Table (1) and indicated by open circles in Figure (7). Thus the coefficients $b_1(T)$, $b_2(T)$, ... $b_6(T)$, $b_7^{(1)}(T)$ and $b_7^{(2)}(T)$ can be used only for $T < T(N_c)$. The properties of $PSV(T)$ for $T > T(N_c)$ will be discussed in the following sections, which deal with "Long Period Extension". The "Short Period Extension" of *PSV* spectral amplitudes for $T < \frac{1}{25}s$ is described in Trifunac and Todorovska [53].

The strong motion acceleration data which served as a basis for this example starts from March 10, 1993, when the first strong motion accelerograms were recorded during the Long Beach (M = 6.3) earthquake in California [55], and extends to the early

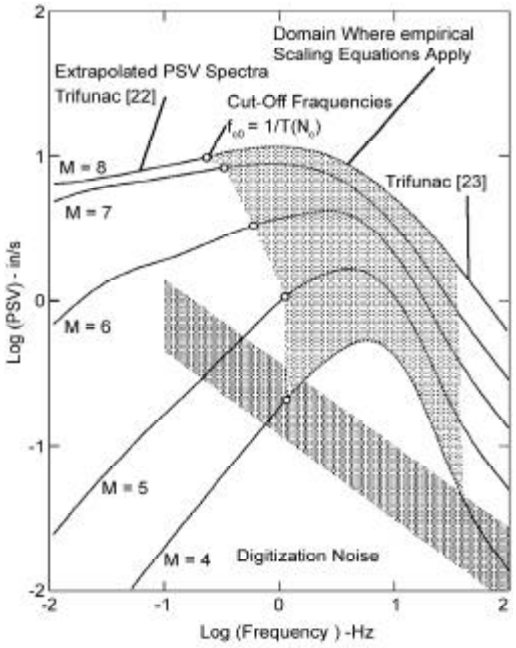

Figure 7. Pseudo relative velocity spectra versus frequency for the MAG-DEPTH model. The spectra are for damping ratio ζ = .05 and probability of exceedance 0.5. The site is at epicentral distance R = 10 km and on rock (h = 0). The source is at H = 5 km depth, and with magnitude M = 4, 5, 6, 7 and 8. Eq. (3.1) is valid inside the light shaded region for frequencies between corner frequency fc0 = 1/T(Nc) and 25 Hz. The periods T(Nc) are defined in Table (1). The extrapolation beyond this zone is as described in this paper. The processing and digitization noise amplitudes are shown by the darker shaded zone increasing from ~10^{-1} to ~1in/sec for frequencies decreasing from 10 to .1 Hz.

Table 1. Cut-Off Period T(N_c) Versus Magnitude.

M	$T(N_c)$	N_c
3	.90	7
4	.90	7
5	1.60	8
6	2.80	9
7	4.40	10
8	7.50	11

1980's. The San Fernando, California earthquake of February 9, 1971, contributed the first major increment to this data. After all accelerograms were digitized, along with selected older recordings between 1933 and 1971, 186 uniformly processed free-field strong motion records became available for study [29,56]. Following the Imperial Valley, in 1979, the Coalinga in 1983, and the Morgan Hill in 1984, earthquakes in California, the uniformly processed strong motion data base more than doubled, to 493 processed records. With recent recordings by the Los Angeles strong motion array (1987 through 1994) and following the Loma Prieta, the Landers, the Big Bear and the Northridge, California, earthquakes, after all this data is uniformly processed, there will be over 2000 excellent region specific records in the strong motion data base, see Figure (2). The exploratory work to determine the local site conditions at all recording stations and the documentation of the results are progressing very slowly. We have been collecting the local soil and the local geologic site parameters since 1975, which are difficult and expensive to obtain on a routine basis. The studies in late 1980's [57,58] could use only 135 sites for which both the local soil and the local geologic data were available. At present, the number of recorded accelerograms with complete site characterization is considerably larger, because of many multiple recordings at the stations where these parameters are available [3].

4. Scaling Parameters

In the above, the principal scaling parameters which describe the empirically determined spectral amplitudes were presented. These parameters are associated with the gray zone illustrated in Figure (7), for frequencies between about .1*Hz* and 25*Hz*. To extend (extrapolate) the $PSV(T)$ amplitudes to long periods $T > T(N_c)$ it is necessary to develop a physical basis for specifying the required extrapolation functions. The physical process involves release of seismic energy at the source, propagation of this energy towards the site (attenuation), and linear dynamic response of a single-degree-of-freedom oscillator.

We begin by considering the linear dimensions of the earthquake source, and assume that the fault surface can be approximated by a rectangle of length, *L*, and width, *W*. Figure (8) (redrawn from [59]) shows the distribution of the "observed" values of *L* and *W* for $2 < M < 8$. The full and dashed straight lines represent W_{min} and L_{min} for one of the fault models used by Trifunac [59] to describe this data in a study of Fourier amplitude spectra of strong motion acceleration. The subscript "min" in L_{min} and W_{min} refers to unilateral faulting and is associated with corner frequencies $f_1 = \left(\frac{L}{2.2} + \frac{W}{6}\right)^{-1}$ and $f_2 = \frac{2.2}{W}$ in the description of spectral amplitudes at long periods ($T > T(N_c)$). In the Fourier space or the response spectrum space, the source dimensions, *L* and *W*, are seen as corner frequencies equal to the inverse of the duration of faulting [60], via dislocation

velocities and wave velocities. For bilateral (symmetric) faulting, for example, when the source spreads from the focus at equal rates in all directions, during the same time, $1/f_1$, twice longer fault will rupture, $L = 2L_{min}$. For bi-lateral faulting, but not with a symmetric spreading rate, we will have $L_{min} < L < 2L_{min}$ and likewise $W_{min} < W < 2W_{min}$. The possible outcomes for L and W are then shown by the grey zones to the right of W_{min} and L_{min} in Figure (8).

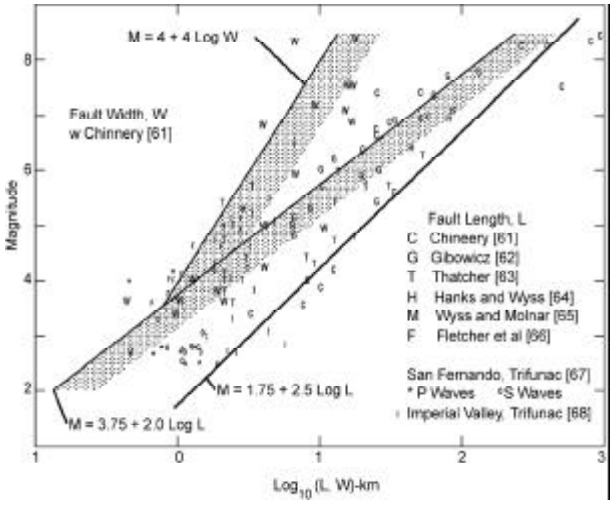

Figure 8. Field and "instrumental" estimates of the fault width (W) and the fault length (L) versus magnitude M. L_{min} and W_{min}, assuming unilateral rupture propagation, are shown by the heavy continuous lines. Symmetrical bilateral faults, with same duration of faulting, would result in two times larger fault dimensions. All other faulting, again assuming the same duration of faulting, falls between these two estimates and is shown by the shaded zones.

Trifunac [59] studied the possible range and the functional forms for L and W, which on one hand must agree with the observational trends in Figure (8) and on the other hand must be consistent with the Fourier spectral amplitudes of recorded strong ground motion in California. Figure (9) illustrates four such models which agree with the data. Table (2) gives the scaling parameters in

$$L_{min} = a \times 10^{bM} \tag{4.1}$$

and

$$W_{min} = c \times 10^{dM} \tag{4.2}$$

or

$$W_{min} = c + fM \tag{4.3}$$

The last expression for W is also equal to the

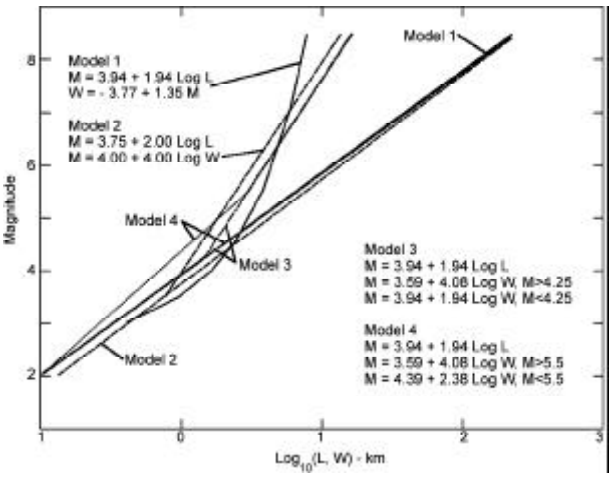

Figure 9. Fault length (L) and fault width (W) versus earthquake magnitude for models 1, 2, 3 and 4, see Table (2).

Table 2. Coefficients a and b in $L_{min} = a \times 10^{bM}$ and c and d in $W = c \times 10^{dM}$.

Fault Length L_{min}				Fault Width W_{min}
Model	a	b	Conditions	$W = \begin{cases} -3.77 + 1.347M & M > 3.1^* \\ .131M & M < 3.1 \end{cases}$
1	.00936	.514	$M > 4.77^*$	
			c d	
2	0.00133	.50	.1 .25	$M > 3.5^*$
			$W = L$ for	$M < 3.5$
3	.00931	.515	.132 .245	$M > 4.25^*$
			$W = L$ for	$M < 4.25$
4	.00931	.515	.132 .245	$M > 5.5^*$
			0.145 .419	$M < 5.5$

* In the text these magnitudes are designated by M^*

"source dimension" S in the attenuation function $Att\ (\Delta, M, T)$, see Eqs. (3.2) through (3.4).

The average relative slip between two sides of a fault is called dislocation, $\bar{u}$. This can be related to the mechanical properties of the material surrounding the source (rigidity, μ, stress released by the faulting, σ, and some representative measure of the size of the fault, say r) by

$$\bar{u} = C_0 \frac{\sigma r}{\mu} \tag{4.4}$$

C_0 can be computed for simple fault geometries analytically, see Table (3), numerically, or can be "estimated" from the regression analyses of strong motion data [69],

$$C_0 \begin{cases} 0.6 & ; M < 4.85 \\ 1.054 - .453M + .0741M^2 & ; 4.85 \le M < 7 \\ 1.52 & ; M \ge 7 \end{cases} \tag{4.5}$$

This C_0 approximates C_0^* discussed by Trifunac

Table 3. Examples of analytical estimates of C_0

$$\bar{u} = C_0 s\, r/m, \qquad \bar{u} = 2\bar{d}$$

Type of Faulting and Fault Geometry	C_0	r Represents
Dip-Slip Displacement along an Infinitely Long Narrow Scrip in a uniform Shear Field [1]	$\frac{3p}{16}$	Fault Width
Infinitely Long Vertical Surface Fault with Strike Slip Displacement [2]	$\frac{p^*}{2}$ to $\frac{p^{**}}{4}$	Fault Width
Circular Fault Plane in an Infinite Medium [3]	$\frac{8}{7p}$	Diameter of Circular Dislocation (Fault Width)

(1) A.T. Star, Slip in a crystal and rupture in a solid due to shear, Cambridge Phil. Society Proc. 24, 489-500 (1928).
(2) L. Knopoff, Energy release in earthquakes, Geophys. J. 1, 44-52, (1958)
(3) V.I. Keilis-Borok [73], on estimation of the displacement in an earthquake source and of source dimensions, Annali Geofizica, 12, 205-214, (1959).
* surface fault
** deep fault

[59,70] and implies a "circular" or a "rectangular" ($L = W$) fault for small M. With increasing M, as L grows faster than W, C_0 also increases, and for $M > 7$ it models very long ($L >> W$) and narrow strike slip faults. It was noted that Eq. (4.5) can be used only for characterization of fault dimensions which are consistent with recorded strong motion accelerograms in Southern California. In other regions where the nature of faulting and the source geometries are different, C_0 will also have to be changed.

The seismic moment M_0 is defined as the product of the material rigidity in the source region, μ, the average dislocation, $\bar{u}$, and the fault area $A = LW$ (or πr^2 for "circular" faults),

$$M_0 = \mu \bar{u} A \tag{4.6}$$

It can be related to the earthquake magnitude empirically or via analysis based on some spectral model of the earthquake source, as

$$log_{10} M_0 = a_m M + b_m \tag{4.7}$$

The coefficient $a_m \sim 1.3$ to 2 and depends on the rate of change of L and W versus magnitude. The coefficient $b_m \sim 11.8 - log_{10}\frac{\eta\bar{\sigma}}{\mu}$, where $\eta\bar{\sigma}$ is the "apparent" stress drop. Typically $b_m \sim 16$ [59,71].

5. Long Period Extension

To extend $PSV(T)$ amplitudes to long periods ($T > T(N_c)$), one must consider two cases, one, for $(R^2 + H^2)^{1/2} >> L$, which will be referred to as "far-field," and the other, for $(R^2 + H^2)^{1/2} < L, W$, which will be called "near-field." To compute $PSV(T)$ at any distance, it will be necessary to specify the weighting functions that measure the relative contribution of the "near-field" and "far-field" terms to the complete ground motion and to the corresponding $PSV(T)$ spectra.

5.1. Far-Field Extension

Let $|_F X_r(T, \zeta)|_{max}$ be the relative maximum response of a single-degree-of-freedom system with frequency $\omega = 2\pi/T$ and fraction of critical damping ζ. To develop a functional form of $|_F X_r(T, \zeta)|_{max}$, which can be used to extend the PSV spectra in the "far-field" beyond $T = T(N_c)$, the Brune's far-field pulse can be used

$$d_F(t) \sim \frac{r}{R}\frac{\sigma\beta}{\mu} t e^{-\alpha t} \tag{5.1}$$

where r represents the source dimension, R is the source to station distance, σ is the Brune's [18] effective stress drop at the fault, β is the velocity of shear waves at the source, and μ is the rigidity of the material surrounding the source. The actual ground motion is more complicated and cannot be described in detail by Eq. (5.1). The advantage of using this simplified representation is in that it is capable of leading to the shape of far-field strong motion Fourier amplitude spectrum which is consistent with many observations [59,72]. By selecting proper scaling parameters, this pulse can be related to the earthquake magnitude (via corner frequency, α). The Fourier amplitude spectrum of $d_F(t)$ in Eq. (5.1) is

$$W_{FF}(\omega) \sim \frac{r}{\mu R}\frac{\sigma\beta}{(\omega^2 + \alpha^2)} \tag{5.2}$$

where $\alpha \approx 2.34\frac{\beta}{r}$ [18]. Assuming that $r \sim W/2$, (W is the fault width) $\alpha/\omega \sim 2.23T/W$. The fault width W can be approximated by

$$W = c \times 10^{dm}, \tag{5.3}$$

where for $M > 3.5$, $c \sim 1$ and $d \sim .25$, see Table (2). Thus, the simple pulse in Eq. (5.1) can be made to be consistent with leading source parameters.

To simplify the notation, while developing the expressions for $|_F X_r(T, \zeta)|_{max}$, we will ignore the amplitude factors $\frac{r}{R}\frac{\sigma\beta}{\mu}$ and will analyze $te^{-\alpha t}$ alone. For ground displacement given by $d_0(T) = te^{-\alpha t}$, the relative response of a single degree of freedom system, x_r, is governed by

$$\ddot{x}_r + 2\omega\zeta\dot{x}_r + \omega^2 x_r = -\left(\alpha^2 t - 2\alpha\right)e^{-\alpha t} \tag{5.4}$$

where the right hand side represents the negative of the second time derivative of $te^{-\alpha t}$. The solution of Eq. (5.4) is

$$x_r(t) = e^{-\omega\zeta t}(a\sin\omega t + b\cos\omega t) + (A + Bt)e^{-\alpha t} \tag{5.5}$$

where, for zero initial conditions $(x_r(0) + d_0(0) = 0;$ $\dot{x}_r(0) + \dot{d}_0(0) = 0)$

$$B = \frac{-\alpha^2}{\alpha^2 - 2\omega\zeta\alpha + \omega^2} \tag{5.6a}$$

$$A = \frac{2\alpha - 2\omega\zeta B + 2\alpha B}{\alpha^2 - 2\omega\zeta\alpha + \omega^2} \tag{5.6b}$$

$$b = -A \tag{5.7a}$$

and

$$a = \frac{\alpha A - B - 1 + b\omega\zeta}{\omega} \tag{5.7b}$$

To find $|_F X_r(T, \zeta)|_{max}$, Eq. (5.5) can be differentiated with respect to time, and by equating this derivative to zero, the maximum for all t can be found. This however leads to lengthy transcendental expressions, which cannot be justified for this simple application. To develop a simple and accurate description of $|_F X_r(T, \zeta)|_{max}$, we use an approximate description of the peak response, by evaluating x_r in Eq. (5.5) at t_{max}/T where t_{max} can be described numerically [53].

Figure (10) shows the logarithm of the normalized (for peak value of the ground displacement $d_F(t)$ equal to one) pseudo relative velocity spectrum *PSV*, which in terms of the dimensionless variables used here is equal to $|_F X_r(T, \zeta)|_{max}(\alpha e)(\omega/\alpha)$, plotted versus $log_{10}[1/(\alpha T)]$ and for five damping values ζ = 0.0, 0.02, 0.05, 0.10 and 0.20. For $\alpha T > 2.34$ the *PSV* spectra of far-field displacement

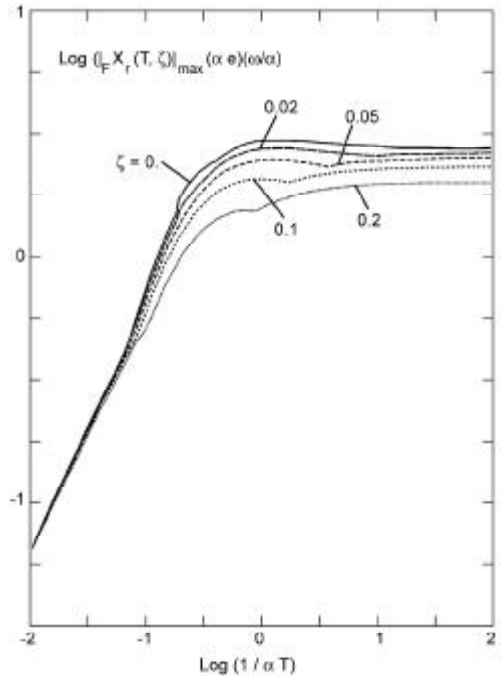

Figure 10. Normalized spectral amplitudes of pseudo relative velocity $|_F X_r(T,\zeta)|_{max}\omega e$, versus dimensionless frequency $[1/(\alpha T)]$ for damping ratios ζ = 0.0, 0.02, 0.05, 0.1 and 0.2. The ground displacement, $d_F(t)$, is the Brune's far-field pulse, having corner frequency α. The normalization is such that $d_F(t)$ has unit peak amplitude.

diminish like $1/(\alpha T)$. For $\alpha T < 2.34$, the *PSV* amplitudes are essentially constant.

To extend the Pseudo Relative Velocity Spectrum *PSV* beyond the period $T(N_c)$, we use the functional form of $|_F X_r(T, \zeta)|_{max}(e\omega)$ and scale it by $d_{F,max}$(= *max* $[d_{FF}(t)]$), $t > 0$, such that at $T = T(N_c)$

$$|_F X_r(T_c, \zeta)|_{max}\frac{2\pi e}{T_c}d_{F,max} = PSV(T_c) \tag{5.8}$$

Then

$$d_{F,max} = \frac{T_c}{2\pi e}\frac{PSV(T_c)}{|_F X_r(T_c, \zeta)|_{max}} \tag{5.9}$$

becomes an estimate of the peak ground displacement at a site, and during an earthquake specified by the arguments used in the description of $PSV(T_c)$, see Eq. (3.1). This $d_{F,max}$ represents an estimate of $\frac{r}{R}\frac{\sigma\beta}{\mu}\alpha e$ and so one can write

$$d_{FF}(t) \sim d_{F,max}\,\alpha e te^{-at} \tag{5.10}$$

The Fourier amplitude spectrum of $d_{FF}(t)$ is

$$W_{FF}(\omega) = d_{F,max}\alpha e\frac{1}{\omega^2 + \alpha^2} \tag{5.11}$$

As $\omega \to 0$, $\Omega_{FF}(\omega) \to M_0/(4\pi\rho R\beta^3)$ [73], where

M_0 is the seismic moment, R is the source to station distance and ρ and β are the density and shear wave velocity in the source region.

Then,

$$d_{F,max} \alpha e \frac{1}{\alpha^2} = \frac{M_0}{4\pi\rho R\beta^3} \tag{5.12}$$

and, since $\beta^2 = \mu/\rho$

$$M_0 = 4\pi\mu R\beta \frac{e d_{F,max}}{\alpha} \tag{5.13}$$

Thus, $d_{F,max}$ from Eq. (5.9) (i.e. from *PSV* spectra in the far-field, at $T = T_c$) can be used to estimate the seismic moment M_0.

Using Eqs. (5.2) and (5.12), we can write

$$\frac{r}{R}\frac{\sigma\beta}{\mu}\frac{1}{\alpha^2} = \frac{M_0}{4\pi\rho R\beta^3} \quad . \tag{5.14}$$

The average dislocation can be expressed as

$$\bar{u} = C_0 \frac{\sigma r}{\mu} \tag{5.15}$$

where C_0 depends on the source geometry and type of faulting, see Eq. (4.5) and Table (3). In the above equations, replacing the "source dimension" r by W, there follows

$$\alpha = 2\beta\left(\frac{\pi}{C_0 L W}\right)^{1/2} \tag{5.16}$$

For C_0=16 / (7π) and for $L W = \pi r^2$ (i.e. circular fault surface) the above expression for α reduces to

$$\alpha = \left(\frac{7\pi}{4}\right)^{1/2}\frac{\beta}{r} \tag{5.17}$$

which is same as the original Brune's [18] corner frequency.

How well $\left|_F X_r(T,\zeta)\right|_{max} e\frac{2\pi}{T_c} d_{F,max}$ can represent the long period *PSV* amplitudes in the far-field can be tested in part by examining how well $d_{F,max}$ computed from Eq. (5.9) and M_0 computed from Eq. (5.13) agree with other independent estimates of the same quantities. Figure (11) shows selected values of peak ground displacements (computed and corrected from the recorded strong motion accelerograms), for magnitudes 6.5 and 7.5 and for distance, R = 200*km*. The three shaded zones in this figure represent $d_{F,max}$ computed from Eq. (5.9) for p = .1, .5 and .9. The width of each grey zone reflects the differences among the members of the *G4RM*. For small distances (R = 10, 20*km*), $d_{F,max}$ underestimates the peak amplitudes of ground displacement of M > 5, but agrees well with data for M < 5 [53]. For R = 200*km*, the trends of $d_{F,max}$ agree well with all recorded data on peak ground displacements.

Figure (12) shows comparison of M_0 computed from Eq. (5.13) with the empirical trend $log_{10} M_0$= 1.45M + 16, for p = .5, ζ = 0 and .2 and at R = 50, 100 and 200*km*. It is seen that the agreement is good.

Related studies of Fourier amplitude spectra [59,70,72] already noted that Eqs. (5.2) and (5.13) result from simplified interpretation of shear wave spectra only, while the empirical equations for *PSV*(T) depend on the complete strong motion signal. Those

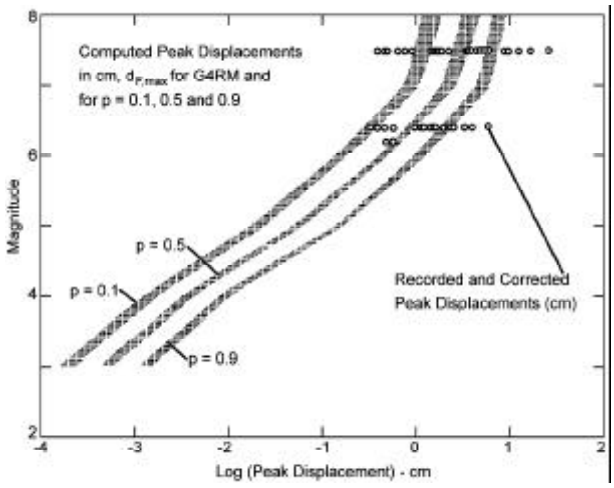

Figure 11. Verification of the long period far-field extension: comparison of peak ground displacement, $d_{F,max}$, computed from Eq. (5.9) for probability of exceedance p = .1, .5 and .9 (the shaded zones) with corrected peak displacements calculated from recorded accelerograms (open circles), at epicentral distance R = 200 km. The shaded zones reflect variations among the G4RM.

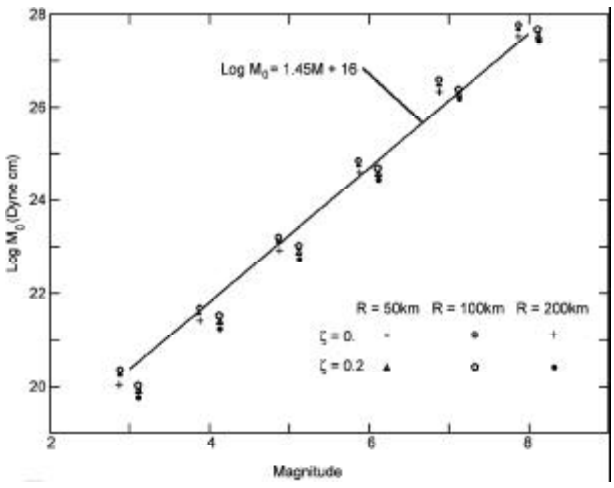

Figure 12. Verification of the long period far-field extension: comparison of $\log_{10} M_0$, computed from Eq. (5.13) (the symbols), with the empirical trend $\log_{10} M_0$ = 1.45M + 16 (solid line). M_0 is the seismic moment.

differences here are corrected approximately by considering the differences between magnitude computed from strong motion data M_L^{SM} [46,47] and the published magnitude representing M_L and M_S (Richter local magnitude for $M_L < 6.5$ and surface wave magnitude for $M_S > 6.5$) via the resulting differences in the empirical equation of Wyss and Brune [71]

$$log_{10}M_0 = 1.45M + 16 \tag{5.18}$$

The details of this correction are described in Trifunac [59].

At present, there is sufficient evidence to require the far-field Fourier amplitude spectra of strong motion to have two corner frequencies. In the related studies of Fourier spectrum amplitudes at long periods [59], spectral shapes with two-corner frequencies have been adopted. Here the shape of $|_F X_r(T, \zeta)|_{max}$ depends on the details of $d_F(t)$ and at present there is no generally accepted and well tested functional form to describe $d_F(t)$ involving two corner frequencies. The pulse used here will nevertheless lead to excellent approximation of *PSV* (T) for $T > 2.34/\alpha$ and may be a rough approximation only when $T < 2.34/\alpha$. However, for the range of earthquake magnitudes 3 to 8, the adopted cut-off periods T_c, see Table (1), are all greater than $2.34/\alpha$ and so it is seen that $d_F(t)$, as in Eq. (5.1), should be an excellent approximation for far-field ground motion pulses, for the intended application in Earthquake Engineering, regardless of whether one-or two-corner frequencies should be considered.

5.2. Near-Field Extension

To find $|_N X_r(T, \zeta)|_{max}$ which can represent the long period PSV spectral amplitudes in the near-field and for periods $T > T_c$, we consider the Brune's [18] characterization of ground displacement near a fault

$$d_N(t) = d_{N,max}\left(1 - e^{-t/\tau}\right). \tag{5.19}$$

$d_{N,max}$ represents the static displacement at a station caused by an earthquake, t is time, and τ is the characteristic time. In reality, the details of ground motion are more complicated, but, for long period oscillators, Eq. (5.19) should give approximate estimates of the relative response.

When the observation point is on the fault surface, the average of $d_{N,max}$ can be related to $\bar{u}$ by

$$\bar{d}_{N,max} \sim \frac{3\bar{u}}{8} \tag{5.20}$$

where $\bar{u}$ is the average dislocation. The characteristic time τ can be approximated by [59]

$$\tau \sim \frac{L}{2.2} + \frac{W}{6} \tag{5.21}$$

where L and W are the fault length and fault width respectively. In the following, we will use $L = L_{min} = a \times 10^{dM}$, and $W = W_{min} = c \times 10^{dM}$, with $a \sim .01$, $b \sim .5$, $c \sim .1$, and $d \sim .25$, see Table (2).

The Fourier transform of Eq. (5.19) is

$$W_{NF}(\omega) = \frac{d_{N,max}}{\tau\omega}\frac{1}{\left(\omega^2 + \tau^{-2}\right)^{1/2}} \tag{5.22}$$

When $\omega \to 0$, $\Omega_{NF}(\omega) \to d_{N,max}/\omega$. To simplify notation, in the following we set $d_{N,max} = 1$ and consider $1 - e^{-t/\tau}$ only.

The relative response, $x_r(t)$, of the single degree of freedom system is then governed by

$$\ddot{x}_r + 2\omega\zeta\,\dot{x}_r + \omega^2 x_r = \frac{1}{\tau^2}e^{-t/\tau} \tag{5.23}$$

The general solution of Eq. (5.23) is

$$x_r(t) = e^{-\omega\zeta t}(a\sin\omega t + b\cos\omega t) + Ae^{-t/\tau} \tag{5.24}$$

Assuming $x_r(0) + d_N(0) = 0$ and $\dot{x}_r(0) + \dot{d}_N(0) = 0$, there follows

$$A = \frac{1}{1 + 2\omega\zeta\tau + (\omega\tau)^2} \tag{5.25a}$$

$$b = -A \tag{5.25b}$$

and

$$a = \left(\frac{1}{\omega\tau} - \zeta\right)A - \frac{1}{\omega\tau}. \tag{5.25c}$$

For small damping (typically $\zeta < .1$) and for small τ/T, the peak relative response occurs at $t = t_{max}$ where $t_{max}/T \sim .5$. For $\zeta > .1$, $t_{max}/T \to 0$.

Figure (13) shows the normalized (for $d_{N,max} = 1$) *PSV* spectra, $PSV \equiv \left|_N X_r(T, \zeta)\right|_{max}(\omega\tau)$, plotted versus $log_{10}(\tau/T)$ and for $\zeta = 0$, 0.02, 0.05, 0.1 and 0.2. For $(\tau/T) < .2$, the *PSV* spectra for near-field displacement diminish like (τ/T). For $(\tau/T) > .2$ the *PSV* amplitudes in Figure (13) are essentially constant.

To extend the *PSV* amplitudes for $T > T_c$ we write

$$\left|_N X_r(T_c, \zeta)\right|_{max}\frac{2\pi}{T_c}\tau\, d_{N,max} = PSV(T_c) \tag{5.26}$$

$$d_{N,max} = \frac{PSV(T_c)}{\left|_N X_r(T_c, \zeta)\right|_{max}}\frac{T_c}{2\pi\tau} \tag{5.27}$$

This $d_{N,max}$ then can be used to scale $\left|{}_N X_r(T,\zeta)\right|_{max}$ beyond $T = T_c$. It also represents an estimate of the permanent ground displacement at a site in the near field where $PSV(T_c)$ has been computed. For $R \rightarrow 0$, that is for an observation point at the fault, the average of $d_{N,max}$ should approach $\bar{u}/2$. To test this, we compute

$$\bar{u} = 2\frac{PSV(Tc)_{R=0}}{\left|{}_N X_r(T_c,\zeta)\right|_{max}}\frac{T_c}{2\pi\tau} \tag{5.28}$$

Figure (14) shows $\bar{u}$ computed from Eq. (5.28), by three grey bands, plotted versus magnitude *M*. The three grey bands correspond to *p* = .1 .5 and .9 (exceedance probabilities), and their widths show fluctuations and differences arising from the *G4RM*. It is seen from Figure (14) that the agreement between $\bar{u}$ computed from Eq. (5.28) and the independent estimates of $\bar{u}$ from other strong motion studies is good.

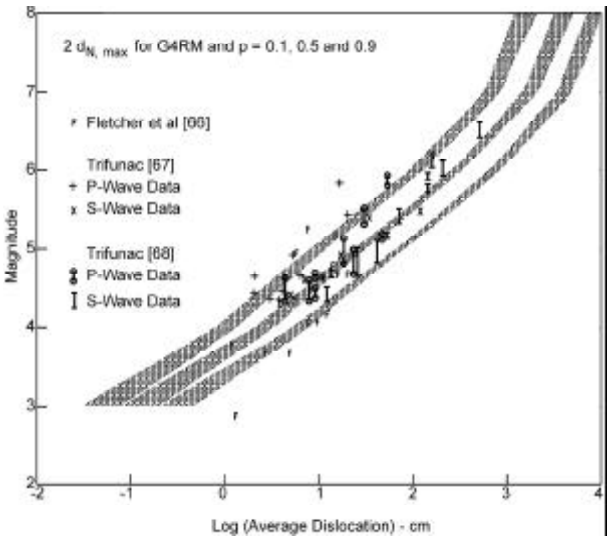

Figure 14. Verification of the long period near-field extension: comparison of $2d_{N,max}$ computed from the G4RM for probability of exceedance p = .1, .5 and .9 (the three shaded zones) with the average dislocation on the fault surface, $\bar{u}$, derived from strong motion studies.

5.3. Transition between Near-Field and Far-Field Spectra

For a continuous transition between $PSV_{NF}(T) \equiv \left|{}_N X_r(T_c,\zeta)\right|_{max}\frac{2\pi}{T}\tau d_{N,max}$ and $PSV_{FF}(T) \equiv \left|{}_N X_r(T,\zeta)\right|_{max} \times e\frac{2\pi}{T}d_{F,max}$ and to complete a representation for use in engineering applications, the results of Jovanovich et al [74,75] was used. They show that the error in representation of the static displacement field by a point source is typically less than 5 percent at distances greater than $4L$, where *L* is the source length. We define the distance S_1, between the station and the "top" of the vertical fault with "dimension" *S*, see Eq. (3.3) and at depth *H* as

$$S_1 = \begin{cases} [R^2 + (H-S)^2]^{1/2}, & H \geq S \\ R, & H < S \end{cases}. \tag{5.29}$$

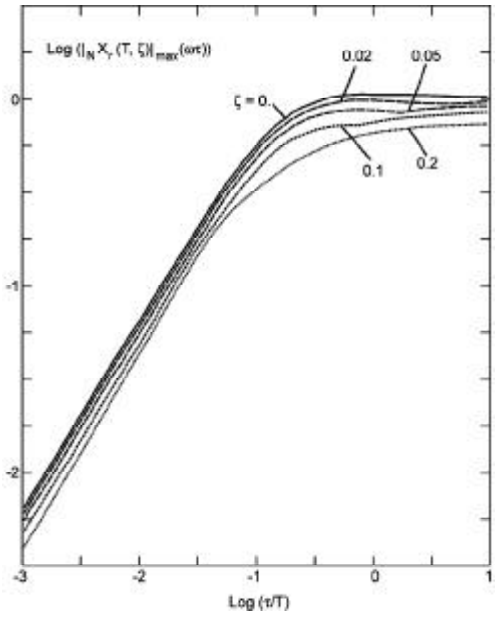

Figure 13. Normalized PSV spectra, $\left|{}_N X_r(T,\zeta)\right|_{max}(\omega\tau)$, plotted versus dimensionless frequency τ/T for ζ = 0, .02, .05, .1 and .2., τ is the characteristic source time, and the displacement, $d_N(t)$, is Brune's near-field displacement. The normalization is such that $d_N(t)$ has unit peak amplitude.

Here, we use $S = 0.01\text{x}10^{.5M}$ when $S \leq 30km$, and $S = 30km$ for larger events, and then combine $PSV_{NF}(T)$ and $PSV_{FF}(T)$ as follows

$$PSV(T) = PSV_{NF}(T)\, e^{-(\frac{3S_1}{4S})} + PSV_{FF}(T)\left(1 - e^{-(\frac{3S_1}{4S})}\right), \quad T > T(N_c) \tag{5.30}$$

In the above expression, 3/4 is used to scale S_1/S so that when S_1/S = 4, the exponent is equal to 3, (so that $e^{-3} = 0.05$), in agreement with the recommendation of Jovanovich et at [74,75]. For $T < T(N_c)$, see Table (1), we use equations of the type illustrated by Eq. (3.1) depending on which of the *G4RM* is used.

For $f < f_{co}\,(=1/T(N_c))$, the heavy solid lines in Figure (7) show $PSV(T)$ computed from Eq. (5.30). For $R = 10km$, $H = 5km$ and $M = 4$ (bottom heavy solid line), since S_1 and Δ are both greater than $4S$, $PSV_{FF}(T)$ contributes mainly to $PSV(T)$, and so $PSV(T) \sim 1/T$.

For $M > 7$, S_1 and Δ are smaller than $4S$, and the amplitudes of $PSV(T)$ shown in Figure (7) are dominated by the flat portion of $\left|{}_N X_r(T,\zeta)\right|_{max} \times e\frac{2\pi}{T} d_{F,max}$, see Figure (13), for T near and shorter than 5τ. For $M = 5$ and 6, the spectra, $PSV(T)$, display progressively changing slope for $f < 1/\tau$. With increasing M (increasing S), this slope decreases from -1 towards 0, as M goes from 4 to 7 and 8, in the period (frequency) range shown in Figure (7).

6. Discussion and Conclusions

The above is based on simplified description and generalization of shear wave spectra of strong ground motion ([18]; Appendix A). This representation does not evolve from a solution of some specific and deterministic source slip, but can be thought of as an intuitive collection of relevant parameters and functional relationships, which by observational understanding of the earthquake source mechanism, and use of dimensional analysis, result in a coherent picture of the main features of strong ground motion. Consequently, our extrapolation of the Pseudo Relative Velocity, $PSV(T)$, of strong ground motion into frequency bands beyond those which can be recorded by currently available strong motion accelerographs is likewise only intuitive and qualitative. Though an effort was made to make as many quantitative tests as possible, we can only hope that the real nature is not too different from these simplified average trends. Yet, the remarkable and encouraging outcome of this exercise is that the various comparisons of our model with independent estimates of seismic moment, peak ground displacements and average dislocation lead not only to good agreements, but also to resolution and scatter which are consistent with other independent estimates.

The largest uncertainties in our extrapolation are believed to exist near $T(N_c)$, where the empirical scaling models approach the recording and processing noise. The tests performed so far suggest that the resulting $PSV(T)$ are probably very realistic for $3.5 < M < 7$ and for horizontal ground motion. The slopes and amplitudes of empirically computed $FS(T)$ and $PSV(T)$ for vertical motions suggest that near $T = T(N_c)$ our empirical models may not be reliable for $M > 6.5$. To understand these amplitudes we need more recorded accelerograms for $M < 7$ and, so, we must patiently wait for this data to become available.

Selection of the low ($f = 1/100Hz$) frequency limits for presentation of all results in this work is arbitrary. Extrapolation of $PSV(T)$ on log - log scale by Eq. (5.30) from $T(N_c)$ towards $T \to \infty$ *s* appears reasonable and agrees favorably with the known trends of seismic moment M_0, peak ground displacements, and of the average dislocation amplitudes, $\bar{u}$, versus earthquake magnitude. Since the corner frequency in Fourier spectrum amplitudes, $1/\tau$, in the near-field ground motion is v/r, where v is the dislocation velocity (typically between 2 and $3km/sec$), and r is the representative source dimension, it is seen that τ can be larger than $T(N_c)$. This is so assuming that, for the frequencies considered here, the rupture occurs as a "smooth" process. Many studies have suggested that the fault slips irregularly, with large dislocations distributed at several or at many "hot" spots, making larger events look like a sequence of smaller events. While this faulting behavior can affect τ appreciably, we do not have at present, reliable data to introduce and to verify such behavior in our analysis.

The "local" nature of strong motion recording, local in the sense of the proximity to the fault (often less than say $100km$), and the fact that it is $\bar{u}$ and not the overall source magnitude or moment and long source dimensions (L) that govern the near-field strong motion amplitudes, all agree with the observed trends of strong motion amplitudes predicted by the *G4RM*.

Numerous further tests and studies of the relationships analogous to Eqs. (5.9), (5.13), (5.16), (5.27) and (5.30) (and of the associated amplitudes, corner frequencies and scaling parameters) are possible. Also, the empirical equations exemplified by Eq. (3.1) can be used to investigate the high frequency attenuation and the trends implied by the peaks of spectral amplitudes for frequencies less than $25Hz$. Many of these studies have been completed in the process of selecting and verifying the physical basis and the equations which are presented in this paper, but their review is beyond the scope of this presentation [38,59,60,69,70,76,77]. The picture which emerges from this work is that of detailed internal consistency and of excellent agreement with near strong ground motion and distant seismological inferences on one hand, and with the theoretical source representations on the other.

References

1. Biot, M.A. (1932). "Vibrations of Buildings during Earthquake", Chapter II in Ph.D. Thesis No. 259 entitled "Transient Oscillations in Elastic System", Aeronautics Department, Calif. Inst. of Tech., Pasadena, California, U.S.A.

2. Benioff, H. (1934). "The Physical Evaluation of Seismic Destructiveness", *Bull. Seism. Soc. Amer.*, **24**, 389-403.

3. Lee, V.W. (2002). "Empirical Scaling of Strong Earthquake Ground Motion – Part I: Attenuation and Scaling of Response Spectra", *Indian Soc. of Earthquake Tech. Journal*, **39**(4), 219-254.

4. Gupta, I.D. (2002a). "The State of the Art in Seismic Hazard Analysis", *Indian Society of Earthquake Technology Journal*, **39**(4), 311-346.

5. Trifunac, M.D. (1988). "Seismic Microzonation Mapping Via Uniform Risk Spectra", *Proc. 9th World Conf. Earthquake Eng.*, **VII**, 75-80, Tokyo-Kyoto, Japan.

6. Trifunac, M.D. (1989c). "Threshold Magnitudes which Exceed the Expected Ground Motion during the Next 50 Years in a Metropolitan Area", *Geofizika*, **6**, 1-12.

7. Trifunac, M.D. (1990a). "A Microzonation Method Based on Uniform Risk Spectra", *Int. J. Soil Dyn. and Earthquake Eng.*, **9**(1), 34-43.

8. Gupta, V.K. (2002b). "Developments in Response Spectrum-Based Response of Structural Systems", *Indian Soc. Earthquake Tech. Journal*, **39**, 347-366.

9. Jordanovski, L.R., M.I. Todorovska, and M.D. Trifunac (1992a). "The Total Loss in a Building Exposed to Earthquake Hazard, Part I: The Model", *Europ. Earthquake Eng.*, **VI**(3), 26-32.

10. Jordanovski, L.R., M.I. Todorovska, and M.D. Trifunac (1992b). "The Total Loss in a Building Exposed to Earthquake Hazard, Part II: a Hypothetical Example", *Europ. Earthquake Eng.*, **VI**(3), 26-32.

11. Suyehiro, K. (1932). "Engineering Seismology Notes on American Lectures", Proc. *ASCE*, **58**(4), 1-110.

12. Kanai, K. (1983). "Engineering Seismology", Univ. of Tokyo Press, Tokyo.

13. Biot, M.A. (1933). "Theory of Elastic Systems Vibrating under Transient Impulse with an Application to Earthquake-Proof Buildings", *Proc. National Academy of Sciences*, **19**(2), 262-268.

14. Biot, M.A. (1934). "Theory of Vibration of Buildings during Earthquakes", Zeitschrift für Angewandte Matematik und Mechanik, **14**(4), 213-223.

15. Biot, M.A. (1941). "A Mechanical Analyzer for the Prediction of Earthquake Stresses", *Bull. Seism. Soc. Amer.*, **31**, 151-171.

16. Biot, M.A. (1942). "Analytical and Experimental Methods in Engineering Seismology", *ASCE* Transactions, **108**, 365-408.

17. Housner, G.W. (1959). "Behavior of Structures during Earthquakes", *J. Eng. Mechanics Division, ASCE*, 85(EM4), p. 109-129.

18. Brune, J.N. (1970). "Tectonic Stress and Spectra of Seismic Shear Waves", *J. Geophys. Res.*, **74**, 4997-5009.

19. Newmark, N.M., Blume, J.A., and Kapur, K.K. (1973). "Seismic Design Criteria for Nuclear Power Plants", *J. Power Division, ASCE*, **99**, 287-303.

20. Seed, H.B., Ugas, C., and Lysmer, J. (1974). "Site- Dependent Spectra for Earthquake-Resistant Design", U.C. Berkeley Report UCB/ EERC-74/12, Berkeley, California.

21. Trifunac, M.D. (1978). "Response Spectra of Earthquake Ground Motion", *ASCE EM5*, **104**, 1081-1097.

22. Trifunac, M.D. (1995a). "Psuedo-Relative Velocity Spectra of Earthquake Ground Motion at Long Periods", *Soil Dynam. Earthq. Engng.*, **14**(5), 331-346.

23. Trifunac, M.D. (1995b). "Pseudo-Relative Velocity Spectra of Earthquake Ground Motion at High Frequencies", *Earthq. Engng. Structural Dynamics*, **24**(8), 1113-1130.

24. Trifunac M.D. and Todorovska, M.I. (2001a). "Evolution of Accelerographs, Data Processing, Strong-Motion Arrays and Amplitude and Spatial Resolution in Recording Strong Earthquake Motion", *Soil Dyn. Earthq. Eng.*, **21**(6), 537-555.

25. Trifunac, M.D. and Todorovska, M.I. (2001b). "A Note on Useable Dynamic Range of Accelerographs Recording Translation", *Soil Dyn. Earthq. Eng.*, **21**(4), 275-286.

26. Trifunac, M.D., Hao, T.Y., and Todorovska, M.I. (2001). "Response of a 14-Story Reinforced Concrete Structure to Excitation by Nine Earthquakes: 61 Years of Observation in the Hollywood Storage Building", Report CE 01-02, Dept. of Civil Eng., Univ. of Southern California, Los Angeles, California, U.S.A.

27. Trifunac, M.D., Udwadia, F.E., and Brady, A.G. (1973a). "Analysis of Errors in Digitized Strong-Motion Accelerograms", *Bull. Seism. Soc. Amer.*, **63**, 157-187.

28. Trifunac, M.D. and Lee, V.W. (1974). "A Note of the Accuracy of Computed Ground Displacements from Strong-Motion Accelerograms", *Bull. Seism. Soc. Amer.*, **64**, 1209-1219.

29. Trifunac, M.D. (1976a). "Preliminary Empirical Model for Scaling Fourier Amplitude Spectra of Strong Ground Acceleration in Terms of Earthquake Magnitude, Source to Station Distance and Recording Site Conditions", *Bull. Seism. Soc. Amer.*, **66**, 1343-1373.

30. Alford, J.L., Housner, G.W., and Martel, R.R. (1964), "Spectrum Analysis of Strong-Motion Earthquakes", *Earthq. Eng. Res. Lab., Calif. Inst. of Tech.*, Pasadena, California, U.S.A. (Originally Published in 1951, Revised in 1964).

31. Housner, G.W. (1970). "Design Spectrum", Chapter 5 in Earthquake Engineering (edited by R.L. Wiegel), Prentice-Hall, New Jersey, U.S.A

.

32. USAEC (1973). "Design Response Spectra for Seismic Design of Nuclear Power Plants", Regulatory Guide No. 1.60, U.S. Atomic Energy Commission, Washington, D.C., U.S.A.

33. Hayashi, S.H., Tsuchida, H., and Kurata, E. (1971). "Average Response Spectra for Various Subsoil Conditions", Third Joint Meeting of U.S. Japan Panel on Wind and Seismic Effects, UJNR, Tokyo, Japan.

34. Seed, H.B., Ugas, C., and Lysmer, J. (1976). "Site Dependent Spectra for Earthquake Resistant Design", *Bull. Seism. Soc. Amer.*, **66**, 221-243.

35. Mohraz, B., Hall, W.J., and Newmark, N.M. (1972). "A Study of Veritcal and Horizontal Earthquake Spectra", AEC Report WASH-1255, N.M. Newmark Consulting Engineering Services, Urbana, Illinois, U.S.A.

36. Gutenberg, B. (1957). "Effects of Ground on Earthquake Motion", *Bull. Seism. Soc. Amer.*, **47**(3), 221-250.

37. Lee, V.W. and Trifunac, M.D. (1995). "Pseudo Relative Velocity Spectra of Strong Earthquake Ground Motion in California", Report CE 95-04, Dept. of Civil Eng., Univ. of Southern California, Los Angeles, California, U.S.A.

38. Trifunac, M.D. (1990b). "How to Model Amplification of Strong Earthquake Motions by Local Soil and Geologic Site Conditions", *Int. J. Earthquake Eng. Struct. Dyn.*, **19**(6), 833-846.

39. Hudson, D.E. (1976). "Strong-Motion Earthquake Accelerograms: Index Volume", Report EERL 76-02, Earthquake Eng. Research Lab., Calif. Inst. of Tech., Pasadena, California, U.S.A.

40. Trifunac, M.D. and Lee, V.W. (1973). "Routine Computer Processing of Strong Motion Accelerograms", Report EERL 73-03, Earthquake Eng. Res. Lab., Calif. Inst. of Tech., Pasadena, California, U.S.A.

41. Lee, V.W. (1989). "Empirical Scaling of Pseudo Relative Velocity Spectra of Recorded Strong Earthquake Motion in Terms of Magnitude, and Both Local Soil and Geologic Site Classifications", *Earthquake Eng. and Eng. Vib.*, **9**(3), 9-29.

42. Lee, V.W. (1990). "Scaling PSV Spectra in Terms of Site Intensity, and Both Local Soil and Geological Site Classifications", *Europ. Earthquake Eng.*, **IV**(1), 3-12.

43. Lee, V.W. (1991). "Correlation of Pseudo Relative Velocity Spectra with Site Intensity, Local Soil

Classification and Depth of Sediments", *Soil Dyn. and Earthquake Eng.,* **10**(3), 141-151.

44. Lee, V.W. (1993). "Scaling PSV from Earthquake Magnitude, Local Soil and Geological Depth of Sediments", *J. Geotech. Eng., ASCE*, **119**(1), 108-126.

45. Richter, C.F. (1958). "Elementary Seismology", *Freeman and Co.*, S. Francisco.

46. Trifunac, M.D. (1991a). M_L^{SM}, *Int. J. Soil Dyn. and Earthquake Eng.,* **10**(1), 17-25.

47. Trifunac, M.D. (1991b). "A Note on the Differences in Magnitudes Estimated from Strong Motion Data and from Wood-Anderson Seismometer", *Int. J. Soil Dyn. and Earthquake Eng.,* **10**(8), 423-428.

48. Gusev, A.A. (1983). "Descriptive Statistical Model of Earthquake Source Radiation and Its Application to an Estimation of Short-Period Strong Motion", *Geophys. J.R. Astr. Soc.*, **74**, 787-808.

49. Trifunac, M.D. and Lee, V.W. (1989a). "Empirical Models for Scaling Fourier Amplitude Spectra of Strong Ground Acceleration in Terms of Earthquake Magnitude, Source to Station Distance, Site Intensity and Recording Site Conditions", *Int. J. Soil Dynam. and Earthquake Eng.*, **8**(3), 110-125.

50. Trifunac, M.D. and Lee, V.W. (1989b). "Empirical Models for Scaling Pseudo Relative Velocity Spectra of Strong Ground Acceleration in Terms of Magnitude, Distance, Site Intensity and Recording Site Conditions", *Int. J. Soil Dyn. and Earthquake Eng.*, **8**(3), 126-144.

51. Trifunac, M.D. and Lee, V.W. (1990). "Frequency Dependent Attenuation of Strong Earthquake Ground Motion", *Int. J. Soil Dynam. and Earthquake Eng.*, **9**(1), 3-15.

52. Trifunac, M.D. and Brady, A.G. (1975). "On the Correlation of Seismic Intensity Scales with the Peaks of Recorded Strong Ground Motion", *Bull, Seism. Soc. Amer.*, **65**, 139-162.

53. Trifunac, M.D. and Todorovska, M.I. (1994). "Broad Band Extension of Pseudo Relative Velocity Spectra of Strong Ground Motion, Dept. of Civil Eng. Report No. CE 94-02, Univ. of Southern California, Los Angeles, California, U.S.A.

54. Amini, A., Nigbor, R.L., and Trifunac, M.D. (1987). "A Note on Noise Amplitudes in Some Strong Motion Accelerographs", *Soil Dyn. and Earthquake Eng.*, **6**(3), 180-185.

55. Hudson, D.E. (1962). "Some Problems in the Application of Spectrum Techniques to Strong-Motion Earthquake analysis", *Bull. Seism. Soc. Amer.*, **52**, 417-430.

56. Trifunac, M.D. (1976b). "Preliminary Analysis of the Peaks of Strong Earthquake Ground Motion-Dependence of Peaks on Earthquake Magnitude, Epicentral Distance and the Recording Site Conditions", *Bull. Seism. Soc. Amer.*, **66**, 189-219.

57. Trifunac, M.D. (1989a). "Dependence of Fourier Spectrum Amplitudes of Recorded Strong Earthquake Accelerations on Magnitude, Local Soil Conditions and on Depth of Sediments", *Int. J. Earthquake Eng. Struct. Dyn.*, **18**, 999-1016.

58. Trifunac, M.D. (1989b). "Empirical Scaling of Fourier Spectrum Amplitudes of Recorded Strong Earthquake Accelerations in Terms of Magnitude and Local Soil and Geologic Conditions", *Earthquake Eng. and Eng. Vib.*, **9**(2), 23-44.

59. Trifunac, M.D. (1993a). "Long Period Fourier Amplitude Spectra of Strong Motion Acceleration", *Soil Dyn. and Earthquake Eng.*, **12**(6), 363-382.

60. Novikova, E.I. and M.D. Trifunac (1994). "Duration of Strong Ground Motion in Terms of Earthquake Magnitude, Epicentral Distance, Site Conditions and Site Geometry", *Earthquake Eng. and Struc. Dyn.*, **23**(9), 1023-1043.

61. Chinnery, M.A. (1969). "Earthquake Magnitude and Source Parameters, *Bull. Seism. Soc. Amer.*, **59**, 1969-1982.

62. Gibowicz, S.T. (1973). "Stress Drop and Aftershocks", *Bull. Seism. Soc. Amer.*, **63**, 1433-1446.

63. Thatcher, W. (1972). "Regional Variations of

Seismic Source parameters in the Northern Baja California", *J. Geophys. Res.*, **77**, 1964-1665.

64. Hanks, T.C. and Wyss, M. (1972). "The Use of Body Wave Spectra in the Determination of Seismic Source Parameters", *Bull. Seism. Soc. Amer.*, **62**, 561-589.

65. Wyss, M. and Molnar, P. (1972). "Efficiency, Stress Drop, Apparent Stress, Effective Stress and Frictional Stress of Denver, Colorado Earthquakes, *J. Geophys. Res.*, **77**, 1433-1438.

66. Fletcher, J., Boatwright, J., Haar, L., Hanks, T., and McGarr, A. (1984). "Source Parameters for Aftershocks of the Oroville, California Earthquake", *Bull. Seism. Soc. Amer.*, **74**, 1101-1123.

67. Trifunac, M.D. (1972a). "Stress Estimates for San Fernando, California Earthquake of February 9, 1971: Main Event and Thirteen Aftershocks", *Bull. Seism. Soc. Amer.*, **62**, 721-750.

68. Trifunac, M.D. (1972b). "Tectonic Stress and Source Mechanism of the Imperial Valley, California, Earthquake of 1940", *Bull. Seism. Soc. Amer.*, **62**, 1283-1302.

69. Trifunac, M.D. (1994c). "Similarity of Strong Motion Earthquakes in California", *Europe Earthquake Eng.*, **VIII**(1), 38-48.

70. Trifunac, M.D. (1993b). "Broad Band Extension of Fourier Amplitude Spectra of Strong Motion Acceleration", Dept. of Civil eng. Report No. CE 93-01, Univ. of Southern California, Los Angeles, California.

71. Wyss, M. and Brune, J.N. (1968). "Seismic Moment, Stress and Source Dimensions for Earthquakes in California - Nevada Region", *J. Geophys. Res.*, **73**, 4681-4694.

72. Trifunac, M.D. (1973). "Analysis of Strong Earthquake Ground Motion for Prediction of Response Spectra", *Int. J. Earthquake Eng. Struct. Dyn.*, **2**(1), 59-69.

73. Keilis-Borok, V.I. (1960). "Investigation of the Mechanism of Earthquakes", *Sov. Res. Geophys.* 4, (Transl. Tr. Geofiz. Inst. 40) Am. Geophys. U. Consultants Bureau, New York.

74. Jovanovich, D., M.I. Husseini, and M.A. Chinnery (1974a). "Elastic Dislocations in a Layered Half Space - I. Basic Theory and Numerical Methods", *Geophys. J.R. Astr. Soc.*, **39**, 205-217.

75. Jovanovich, D., M.I. Husseini, and M.A. Chinnery (1974b). "Elastic Dislocation in a Layered Half Space-II: Point Source", *Geophys. J. Royal Astr. Soc.*, **39**, 219-239.

76. Trifunac, M.D. (1994a). "Fourier Amplitude Spectra of Strong Motion Acceleration: Extension to High and Low Frequencies", *Earthquake Eng. Struc. Dyn.*, **23**(4), 389-411.

77. Trifunac, M.D. (1994b). "Q and High Frequency Strong Motion Spectra", *Soil Dyn. and Earthquake Eng.*, **13**(3), 149-161.

78. Brune, J.N. (1968). "Seismic Moment Seismicity and Rate of Slip along Major Fault Zones", *J. Geoph. Res.*, **73**, 777.

79. Von Kármán, T. and Edson, L. (1967). "The Wind and Beyond", Little, Brown and Co., Boston, U.S.A.

80. Von Kármán, T. and Biot, M.A. (1940). "Mathematical Methods in Engineering", McGraw-Hill, New York, U.S.A.

81. Biot, M.A. (1965). "Mechanics of Incremental Deformation", John Wiley and Sons, New York, U.S.A.

82. Biot, M.A. (1970). "Variational Principles in Heat Transfer", Clarendon Press, Oxford, U.K.

Appendix A

Relative Significance of Brune's [18] Paper*- Analysis of Citations

The impact of the published work of scientists is increasingly being assessed on the basis of the number of times their work is cited. This quantitative measure is derived from the Science Citation Index database developed by the Thomson Institute for Scientific Information (*ISI*) (http://www.isinet.com), 3501 Market Street, Philadelphia, PA 19104.

Between 1959 and early 2004 Brune published 200 articles (4.35/year—normal count; or 1.92/year—per-author count), of which 154 were journal papers

(3.42/year—normal count; or 1.55/year—per-author count), in a steady and continuous manner, as shown in Figure (A.1). The "normal count" gives full credit to all contributors regardless of the order of the listed authors. The "per-author count" gives each author credit equal to $1/a_i$, where a_i is the number of authors. Figure (A.2) compares Brune's cumulative number of publications (normal count) with those of 18 Professors of Earthquake Engineering in the U.S., a subset of a sample of 52 faculty studied by Trifunac and Lee [A.1]. The letter codes in this figure indicate institutions where these professors work (CIT—California Institute of Technology, SU—Stanford University, UCB—Univ. Cal. Berkeley, UCSD—Univ. Cal. San Diego, USC—University of Southern Cal., and UCI—Univ. Cal. Irvine), and the numerals correspond to individual faculty members.

A complete and detailed analysis of Brune's citations is beyond the scope of this Appendix. The modern *ISI* database [A.1] contains only citations from papers written after 1975, and since Brune started to publish in 1959 only a subset of all of his citations—received between 1975 and 2004—has been included here. Figure (A.3) shows the number of citations of Brune's papers in the ISI database plotted against years when the cited papers were published. It shows that most of his citations come from two papers, written in 1968 and 1970. Between 1975 and June 8, 2004 Brune accumulated 4,451 citations in the *ISI* database, or 156 citations per year on average. His most cited paper, "Tectonic Stress and Spectra of Seismic Waves from Earthquakes", see Figure (A.3), published in 1970, reached 1,134 citations in June 2004 (with 40 citations per year). Further analysis of who cited this paper shows that about 57% of citations

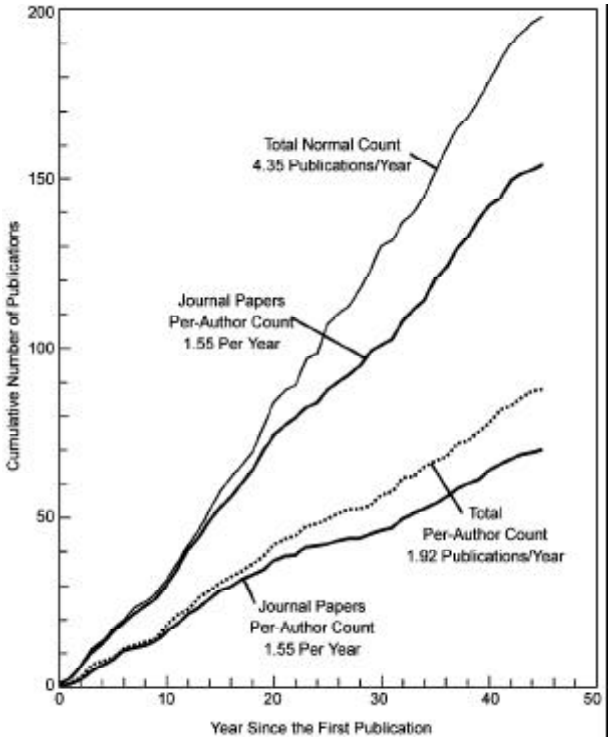

Figure A.1. Cumulative Number of Publications of J.N. Brune versus time (in years since the first publication).

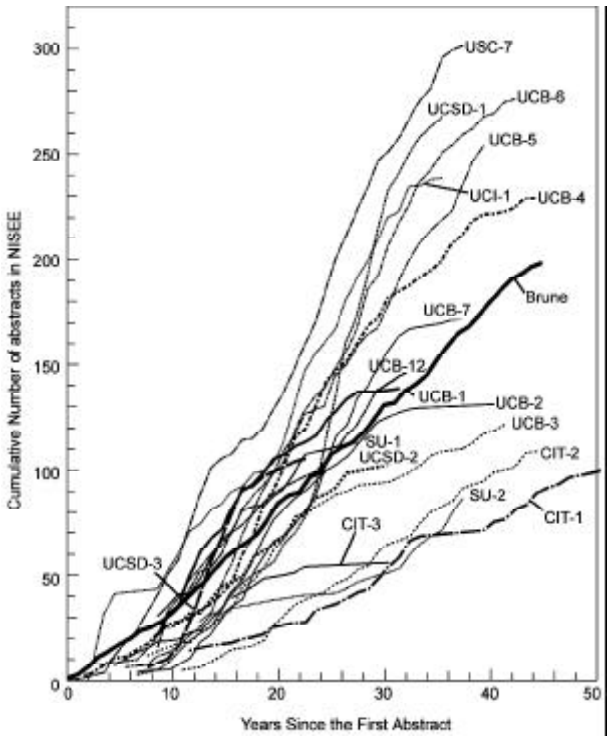

Figure A.2. Comparison of the cumulative number of published articles in the National Information Service for Earthquake Engineering (NISEE) database versus time (in years since the first citation) for 18 faculty in earthquake engineering with cumulative number (normal count) of publications of J.N. Brune.

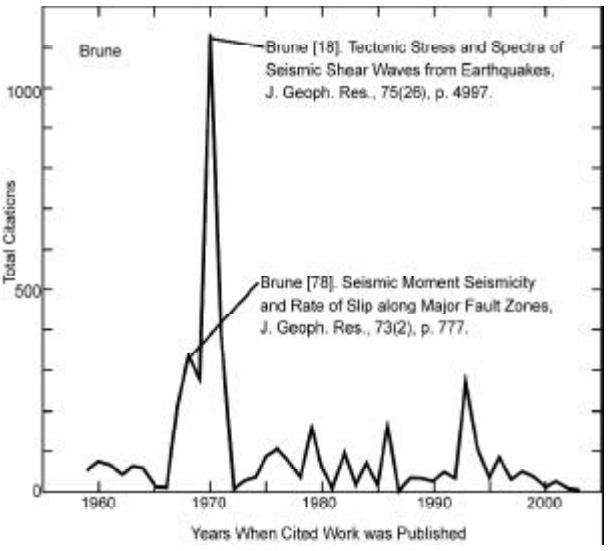

Figure A.3. Total ISI citations of J.N. Brune versus his age at the time his cited work was published.

come from authors who cited it only once, while 25% come from 38 authors (listed in Figure (A.4) who cited the paper more than five times.

It is clear and well known that Brune's impact in several subject areas of geophysics and earthquake engineering is exceptional. The fact that the number of citations his papers received in these areas is also high supports and reinforces ISI's hypothesis that counting citations can be a measure of the impact of a researcher's published work [A.2]. I hope that this simple analysis of the citations of Brune's papers will inspire and influence young and future researchers to focus on quality, substance, and original ideas.

Authors who Cited Brune [18]
(1134 Citations as of June 2004)

Number of Citations	Number of Authors	Cumulative Citations	Cumulative Percent	
16	1	16	1.6	Atkinson
14	1	31	3.0	McGarr
13	1	44	4.2	Boatwright
12	1	56	5.4	Frankel
11	1	67	6.4	Anderson
10	3	97	9.3	Boore, Gibowicz, Singh
9	2	115	11.0	Hough, Hanks
8	7	171	16.4	Fletcher, Hartzell, Klyuchevski, Langston, Lomnitz, Sokokov, Trifunac
7	7	185	17.7	Abercombie, Beresnev
6	5	215	20.6	Aki, Bakun, Kanamori, Rebollar, Sherbaumaum
5	9	260	25.0	Archuleta, Caputo, Castro, Hwang, Herrman, Madariaga, Papageorgiou, Taylor, Zollo
4	8	292	28.0	
3	18	346	33.1	
2	53	452	43.3	

592 Authors Cited Brune [18] Once, Contributing 56.7%
to the Total of 1134 Citations

Figure A.4. Number of citations, Number of authors, cumulative citations, and cumulative percentage of 1134 citations, in June 2004, for authors who cited Brune [12] more than five times.

References

A.1. Trifunac, M.D. and Lee, V.W. (2004). A Study of the Relative Ranking of Twelve Faculty of the USC Civil Engineering Department—Experiments with Scientific Citations Index Expanded, Dept. of Civil Engineering, Report CE-04-03, University of Southern California, Los Angeles, California.

A.2. Trifunac, M.D. (2005). "Scientific Citations of M.A. Biot", Third Poromechanics Conference, *Biot Centennial (1905-2005)*, Abousleiman, Y.N., Cheng, A.H-D., and Ulm, F-J. (editors), A.A. Balkema Publishers, Taylor and Francis Group plc, London, England, 11-17.

---

* James N. Brune is Professor of Geophysics, Seismological Laboratory and Dept. of Geol. Sciences, Mackay School of Mines, University of Nevada, Reno. This Appendix was written on the occasion of his 70th birthday by his former graduate student, with gratitude for his guidance and inspiration.

Endnotes

1. Theodore von Kármán, born in Budapest, Hungary (1881-1963), engineer, applied scientist, teacher and visionary, was the first director of the Daniel Guggenheim Graduate School of Aeronautics at the California Institute of Technology, where he arrived in 1930 from Aachen, Germany. Von Kármán had foresight, creativity, and a remarkable talent for getting people together across professional, national, and language barriers. He was one of the foremost leaders in the world of aviation and space technology [79].

2. Maurice A. Biot, born in Antwerp, Belgium (1905-1985), was an engineer, physicist, and applied mathematician. After graduating in electrical and mining engineering and philosophy, and receiving his D.Sc. degree (1931) from the University of Louvain (Belgium), he went to Caltech, where he received a Ph.D in 1932, in Aeronautical Sciences. He was a student and then collaborator of Theodore von Kármán with whom he wrote a classical textbook "Mathematical Methods in Engineering" [80]. He taught briefly at Louvain, Harvard, Columbia, Caltech, and Brown Universities. As an independent scientific consultant, he worked for Shell Development, Cornell Aeronautic Laboratory, and Mobil Research. Biot published 179 articles, three books [80,81,82], and he was holder of seven patents. A man of great and unique talent, Biot worked without students and essentially alone.